

RESEARCH ACTIVITIES V

Department of Applied Molecular Science

V-A Synthesis of Chiral Molecule-Based Magnets

Construction of molecule-based magnetic materials, which have additional properties such as conductivity or photo reactivity, is now becoming a challenging target. Specific goals aimed for these molecule-based magnets include: i) the ability to design the molecular building blocks and to organize them in the solid for desired dimensionality, ii) the optical transparency. The physical characteristic of current interest involves optical properties, particularly with respect to natural optical activity. When a magnet has optical transparency and chiral structure, the magnetic structure of crystal expects to be a chiral spin structure. These magnets will show an asymmetric magnetic anisotropy and magneto-chiral dichroism⁴. This category materials don't only have scientific interest but also have the possibility for use in new devices. When we construct chiral molecule-based magnets, chirality must be controlled not only in the molecular structure, but in the entire crystal structure. As a consequence of this difficulty, only few examples of this type of magnet exist. Up to the present reported chiral magnets have low dimensional magnetic structures, the magnetic ordering temperatures are below 10 K. To afford a high- T_C magnet, dimensionality of magnetic structure must be extended in two or three dimension. When we introduce magnetic bricks, which have more than three connections for the construction of magnets, we can expect to make two or three-dimensional magnets. To make high dimensionality molecule-based magnets, we recently discovered using cyano bridged complex with chiral organic ligands.

V-A-1 Structure and Magnetic Properties of a Chiral Two-dimensional Ferrimagnet with T_C of 38 K

INOUE, Katsuya; KIKUCHI, Koichi¹
(¹IMS and Tokyo Metropolitan Univ.)

Synthesis, magnetic properties and structure of new chiral, transparent, high $T_C = 38$ K molecule-based two-dimensional ferrimagnet, $[\text{Cr}(\text{CN})_6][\text{Mn}(\text{S})\text{-pnH}(\text{H}_2\text{O})](\text{H}_2\text{O})$; ((*S*)-pn = (*S*)-1,2-diaminopropane) are described. The complex was obtained as green needle crystal by the reaction of $\text{K}_3[\text{Cr}(\text{CN})_6]$, $\text{Mn}(\text{ClO}_4)_2$, and (*S*)-1,2-diaminopropane dihydrochloride ((*S*)-pn·2HCl) in 1:1:1 molar ratio in methanol/ H_2O (1:1) solution under argon atmosphere (adjusted pH 6–7 by KOH). X-ray structural analysis revealed a crystallized chiral space group of Orthorhombic, $P2_12_12_1$; moreover, the complex demonstrated a two-dimensional magnetic network. The magnetic measurements of the complex show Mn^{II} and Cr^{III} ions interact ferrimagnetically and magnetic transition occurs at 38 K.



Figure 1. A single crystal of a chiral molecular ferrimagnet, $[\text{Cr}(\text{CN})_6][\text{Mn}(\text{S})\text{-pnH}(\text{H}_2\text{O})](\text{H}_2\text{O})$.

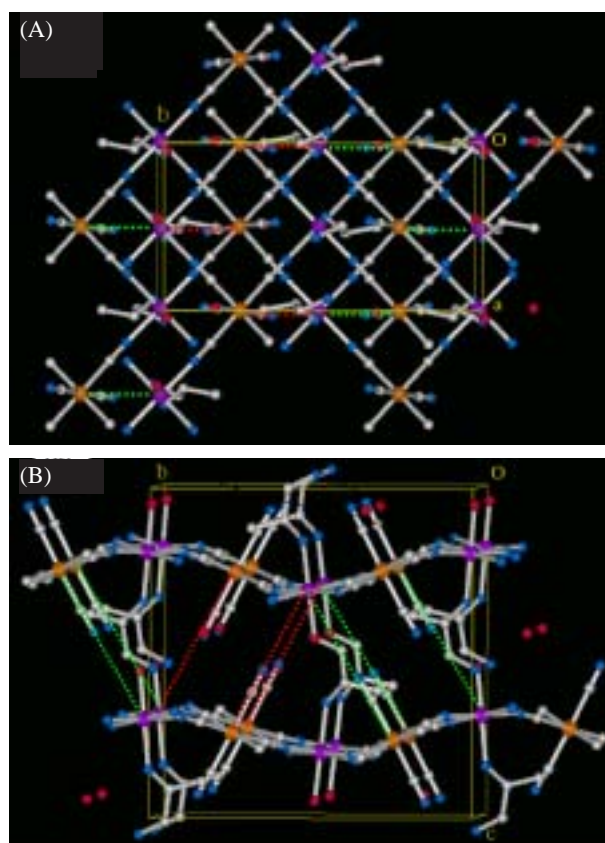


Figure 2. Crystal structure of $[\text{Cr}(\text{CN})_6][\text{Mn}(\text{S})\text{-pnH}(\text{H}_2\text{O})](\text{H}_2\text{O})$. (A) Projection onto the ab plane. (B) Projection onto the bc plane.

V-B Hydrothermal Synthesis of Molecule-Based Magnets

Coordination polymers are attracting much interest due to the strength and rigidity of the extended lattices for gas absorption and intercalation and for the connectivity between magnetic ions in designing molecule-based magnets. They belong to a subset of organic-inorganic hybrid materials, and usually employ a central metal ion and a multitopic organic ligands or a coordination complex having ambidentate ligands, such as cyanide and oxalate. In some cases, other organic ligands are used to control the dimensionality or structure. The choice of the metals and of the ligands depends on the desired properties. On the one hand, there is strong interest by scientists studying catalysis and the absorption of gases originating from the possibility of creating structures with cavities, channels or pores and, consequently, large surface areas. On the other hand, there is increasing interest from magneto-chemists due principally to the realization of organizing the magnetic orbitals of the moment carriers to favor a particular magnetic ground state. The field of coordination polymers based on organic radicals is a very active area, indeed. Several ground states have been established and a clear molecular-orbital picture to explain the observations is emerging. For the realizing strong magnetic interaction, it is better to use simple and small organic ligands, such as cyanide or carboxylate ions. The metal complexes with such ligands are usually less solvability. The thermal synthesis is powerful method to make large single crystals for such complexes.

V-B-1 Self-Organized Metallo-Helicates and –Ladder with 2,2'-Biphenyldicarboxylate ($C_{14}H_8O_4$)²⁻: Synthesis, Crystal Structures, and Magnetic Properties

KUMAGAI, Hitoshi¹; INOUE, Katsuya; KURMOO, Mohamedally¹

(¹IMS and Inst. Phys. Chem. Materials Strasbourg, France)

We report on the hydrothermal synthesis, single-crystal structures and magnetic properties of three one-dimensional coordination polymers employing the 2,2'-biphenylcarboxylate dianion, ($C_{14}H_8O_4$)²⁻, as the

bridging component. [$M^II(H_2O)_4(C_{14}H_8O_4)$], where $M = Co$ and Ni , consist of helical chains of square-planer $M^II(H_2O)_4$ bridged by $C_{14}H_8O_4$ with each carboxylate group acting as a mono-dendate ligand. The magnetic properties are those of paramagnets with an antiferromagnetic exchange for Co complex and a ferromagnetic exchange for Ni complex. $Cu(C_{14}H_8O_4)(H_2O)_2$ is composed of tetracarboxylato-dimeric units bridged into ladders by biphenyl units. The ladders are packed parallel to each other, and narrow channels are present due to insufficient space filling of the biphenyl rings. Its magnetic behavior follows that of a Bleaney-Bowers singlet-triplet model with a gap of 470 K.

V-C Synthesis and Characterization of Quantum-Spin Systems

There has been considerable current interest in the study of a low-dimensional quantum-spin system with an energy gap. For such study, organic radicals will provide good examples of ideal Heisenberg spin systems, since they consist only of light elements. By the appropriate design of molecules, we can obtain a variety of spin systems. In these years, we focus on the spin-ladder system, which is interesting in terms of Haldane state and the high T_C superconductivity. For the $S = 1/2$ Heisenberg spin ladder with antiferromagnetic legs and rungs, the ground state of the resonating valence bond (RVB) state or the dimerized state is theoretically expected. Experimentally, the singlet ground state was observed in some ladder systems formed by Cu-based compounds. The study of spin ladder systems has been mainly devoted to that of $S = 1/2$, but that of $S = 1$ is also interesting. We have succeeded in synthesis of the first example of a spin ladder system of $S = 1$ by BIP-TENO. Peculiar properties are observed and theoretical study is also activated.

V-C-1 Magnetic Properties of Organic Two-Leg Spin Ladder Systems with $S = 1/2$ and $S = 1$

KATOH, Keiichi¹; HOSOKOSHI, Yuko; INOUE, Katsuya; BARTASHEVICH, M. I.²; NAKANO, Hiroki³; GOTO, Tsuneaki²

(¹GUAS; ²Univ. Tokyo; ³Himeji Inst. Tech.)

Magnetic properties of spin systems on the two-leg ladder made of organic radicals are studied. The magnetization measurements below 4.2 K in pulsed magnet fields up to about 50 T were done for BIP-BNO as an $S = 1/2$ ladder and for BIP-TENO as an $S = 1$ ladder. An energy gap above the singlet ground state is observed in each compound. Experimental results of magnetizations and susceptibilities are understood from the analysis using the results of the numerical diagonalizations.

[*J. Phys. Chem. Solids* **63**, 1277 (2002)]

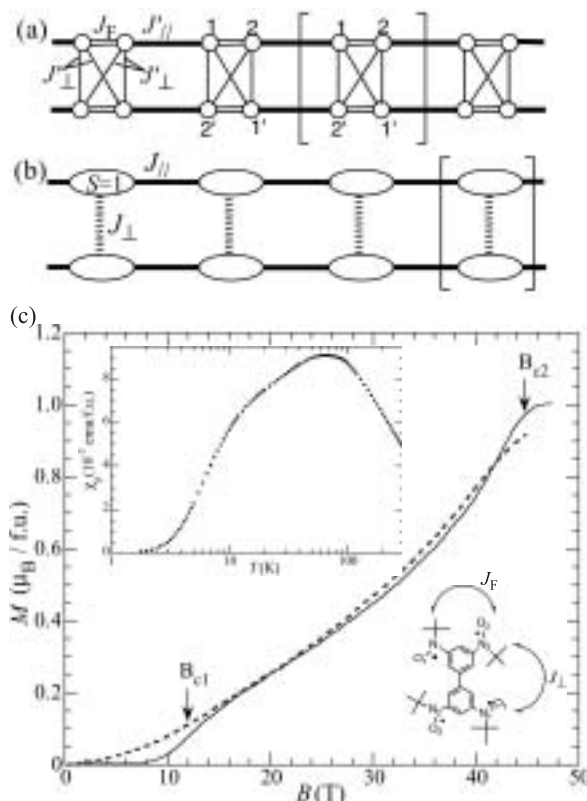


Figure 1. Magnetic exchange coupling scheme in BIP-TENO crystals. A circle and a bond represent an $S = 1/2$ and the exchange coupling, respectively: J_F and J_{\perp} correspond to intramolecular exchange couplings and J_{\parallel} is intermolecular one. (b) Extreme limit of the model (a) when $J_F \rightarrow \infty$. (c) Magnetization curves of BIP-TENO in pulsed high magnetic fields. Solid and dotted curves are the results for 1.7 and 4.2 K, respectively. Inset: Temperature dependence of the paramagnetic susceptibility of BIP-TENO.

V-C-2 Low Dimensionality Observed by ESR Measurements in $S = 1$ Spin Ladder Substance BIP-TENO

OHTA, Hitoshi¹; KIRITA, Keizo¹; KUNIMOTO, Takashi¹; OKUBO, Suzumu¹; HOSOKOSHI, Yuko; KATOH, Keiichi²; INOUE, Katsuya; OGASAWARA, Akira³; MIYASHITA, Seiji³
(¹Kobe Univ.; ²GUAS; ³Univ. Tokyo)

[*J. Phys. Soc. Jpn.* **71**, 2640 (2002)]

X-band ESR measurements of BIP-TENO single crystal, which is an $S = 1$ spin ladder model substance, have been performed in the temperature region from 3.5 to 300 K. At room temperature, the angular dependences of g -value and line width were observed. The line shape and the angular dependence of the line width showed the typical behavior of the low dimensional antiferromagnet. The temperature dependence measurements showed the minimum of the line width and the dynamical g -shift, which were also the typical behavior of the low dimensional antiferromagnet. However, the direction of the dynamical g -shift does not coincide with the well known Nagata's theory, and the comparison with the recent direct ESR calculation by Miyashita *et al.* is discussed.

V-D Organic Ferrimagnetism

In the last decades, the magnetism of molecule-based material has drawn much interest. After the discovery of the organic ferromagnet in 1991, search for an organic ferrimagnet attracts great interest and is considered as one of today's challenging targets in material science. Although a number of ferrimagnets are realized in inorganic-organic hybrid systems, a genuine organic ferrimagnet has not yet been realized. In 1980's, ferrimagnetism is proposed as an effective strategy to give organic materials spontaneous magnetizations by the alternant arrangement of two kinds of organic radicals having different spin-multiplicities. All the reported ferrimagnets include at least two magnetic components: bimetallic compounds or metal complexes with organic radicals. In order to achieve this challenging subject of an organic ferrimagnet from a different viewpoint, we propose here a single-component strategy: utilizing a triradical including an $S = 1$ and an $S = 1/2$ units within a molecule and connecting the $S = 1$ and $S = 1/2$ units by intra- and intermolecular antiferromagnetic interactions. Our new strategy to use a single component has the advantages of the easiness of controlling the crystal structure and the good crystallinity for quality and size.

V-D-1 Magnetic Properties on an Organic Ferrimagnetic Compound and Related Materials

HOSOKOSHI, Yuko; KATOH, Keiichi¹; INOUE, Katsuya
(¹GUAS)

[*Synth. Met.* in press]

Search for an organic ferrimagnet has been one of the challenging targets in the field of material science. Recently, we have reported the successful results for the crystals of a novel organic triradical of PNNBNO, 2-[3',5'-bis(*N*-*tert*-butylaminoxy)phenyl]-4,4,5,5-

tetramethyl-4,5-dihydro-1*H*-imidazol-1-oxyl 3-oxide. This is the first example of a genuine organic ferrimagnetic material having well-defined chemical and crystal structure with $T_C = 0.28$ K. The properties of PNNBNO are described and the magnetic interactions of this system are discussed in comparison with the related oligoaminoxyl.

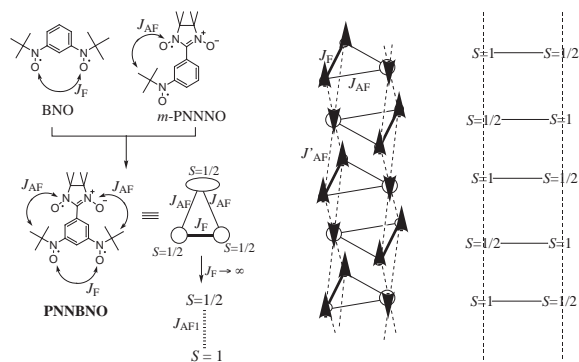


Figure 1. Scheme of the single component strategy for organic ferrimagnetism.

V-E Pressure Effects on Molecular Magnetism

'Pressure' is a powerful tool to control the molecular packings and physical properties. The molecule-based materials with small densities are 'soft' and can be expected to show large pressure effects. For the magnetic measurements with high-accuracy, we have developed a small high-pressure clamp cell made of non-magnetic Cu-Ti alloy which can be equipped to a Quantum Design SQUID magnetometer for the *dc* and *ac* magnetic measurements. The inner pressure of the clamp cell has been calibrated by the superconducting transition temperature of Pb. We have already discovered that some kind of structural change can be suppressed by pressurization. We are now studying the pressure effects on the molecule-based magnetic materials in wider range. In molecular materials, the spin density are delocalized and distributed in a molecule and the spin-density-distribution plays an important role in the exchange interactions. It is attractive to control the sign of the exchange coupling by pressurization. The pressure effects on the related compounds with similar crystal structures are studied.

V-E-1 Pressure Effects on Molecular Magnets of Mn Complexes with Bisaminoxylbenzene Derivatives

SUZUKI, Kentaro¹; HOSOKOSHI, Yuko; INOUE, Katsuya
(¹GUAS)

[*Mol. Cryst. Liq. Cryst.* **379**, 247 (2002)]

Pressure effects on the magnetic properties of a series of quasi-one-dimensional molecular magnets have been studied. The complexes of Mn(hfac)₂ (hfac = hexafluoroacetylacetonate) with 1,3-bis(*N*-*tert*-butylaminoxyl)benzene and its 5-halo- derivatives, abbreviated as **1_X** (X = H, F, Cl and Br), have almost the same ferrimagnetic chain structure. The difference is seen in the interchain molecular arrangement. The complexes of **1_H** and **1_F** are metamagnets with weak interchain antiferromagnetic interactions, whereas **1_{Cl}** and **1_{Br}** are ferrimagnets with weak interchain ferromagnetic interactions. In two metamagnets (**1_H**, **1_F**), the pressurization simply results in the enhancement of the interchain antiferromagnetic interactions, which is reflected by the higher transition temperature and spin-flipping field. On the other hand, in the ferrimagnet (**1_{Cl}**), the metamagnetic behavior is observed under pressure. It is suggested that the subtle change of the relative arrangement of chain structures affects the interchain ferromagnetic interactions.

V-E-2 Pressure-Induced Metamagnetic Behavior in a Quasi-One-Dimensional Molecule-Based Ferrimagnet

SUZUKI, Kentaro¹; HOSOKOSHI, Yuko; INOUE, Katsuya
(¹GUAS)

[*Chem. Lett.* 316 (2002)]

Pressure effects on a molecule-based ferrimagnet of [Mn(hfac)₂](Br-BNO) (**1_{Br}**) were studied, where hfac = hexafluoroacetylacetonate and Br-BNO = 5-bromo-1,3-bis(*N*-*tert*-butylaminoxyl)benzene. At ambient pressure, **1_{Br}** is a ferrimagnet with $T_C = 5.4$ K. We observed the metamagnetic behavior of **1_{Br}** under pressure.

V-F Bioinorganic Studies on Structures and Functions of Non-Heme Metalloenzymes Using Model Complexes

Metal-containing enzymes have been widely distributed in both plants and animals and have been related to metabolic processes such as hydroxylation, oxygen transport, oxidative catalysis, electron transfer, and so on. In this project, their structural/functional models have been originally constructed and studied using physico-chemical methods.

V-F-1 Novel Phosphate Bond Formation in a Cobalt(III) Complex System

FUNAHASHI, Yasuhiro¹; YONEDA, Atsuro¹;
TAKI, Chiyo¹; OZAWA, Tomohiro¹;
JITSUKAWA, Koichiro¹; MASUDA, Hideki²
(¹Nagoya Inst. Tech.; ²IMS and Nagoya Inst. Tech.)

[*Inorg. Chem.* submitted]

Reaction of an aqueous solution (pH 3) of [Co^{III}(tpa)(CO₃)]Cl (**1**) (tpa = tris(2-pyridylmethyl)amine) with 2 equiv. of an active phosphate ester, disodium 4-nitrophenylphosphate (NPP), in the presence of a catalytic amount of active charcoal at 60 °C gave [Co^{III}(tpa)(PO₄)] (**2**) (7.8% yield) and [{Co^{III}(tpa)}₂(μ-P₂O₇)]Cl₂ (**3**) (50.7% yield). The structures of **2** and **3** were determined by X-ray crystallography. Complex **3** has a novel molecular structure with ligation of the two Co(III) centers *via* an NPP-derived bridging-diphosphate. The phosphate bond formation does not occur without active charcoal or under conditions of neutral pH. A proposed reaction mechanism involves initiation by hydrolysis of NPP to give **2** with the phosphate bond formed as an intermediate dimer structure.

V-F-2 Syntheses and Structures of Tetrakis(1-methyluracilato)palladium Complexes Capturing Alkali Metal Ions. A New Type of Metallo-Podand

MIZUTANI, Mamoru¹; MIWA, Satoshi^{1,2};
FUKUSHIMA, Nobuhiro^{2,3}; FUNAHASHI,
Yasuhiro¹; OZAWA, Tomohiro¹; JITSUKAWA,
Koichiro¹; MASUDA, Hideki⁴
(¹Nagoya Inst. Tech.; ²SIGI Japan; ³Collaboration Lab.;
⁴IMS and Nagoya Inst. Tech.)

[*Inorg. Chim. Acta* in press]

Four tetrakis(1-methyluracilato)palladium complexes containing alkali metal ions, [Li₂Pd(1-MeU⁻)₄] (**1**), [Na₂Pd(1-MeU⁻)₄] (**2**), [K₂Pd(1-MeU⁻)₄] (**3**), and [Cs₂Pd(1-MeU⁻)₄] (**4**), have been prepared from M₂PdCl₄ (M = Li⁺, Na⁺, K⁺, and Cs⁺) and four equivalents of 1-methyluracil (1-MeUH). The X-ray crystal structure analyses of complexes **2**, **3** and **4** have revealed that each palladium atom is coordinated in a square-planar geometry with four 1-MeUH-derived N3-deprotonated imidato groups, upright-oriented with angles of 60 ~ 70° from the basal coordination plane. Interestingly, the carbonyl groups of the four imidato rings form two cavities above and below the Pd(II) atom, and two alkali

metal ions are incorporated with Pd–M distances of 3.007(4) and 3.137(3) Å for **2**, 3.432(3) and 3.594(3) Å for **3**, and 3.746(1) and 3.999(1) Å for **4**, respectively. The cavity sizes of the three complexes are tunable according to the ionic radii of the alkali metal ions. ¹H-NMR spectra of complexes **1–4** indicate that all proton signals of the 1-MeU⁻ moiety shifted upfield relative to those of free 1-MeU⁻. The magnitude of the up-field shifts, **1** < **2** < **3** < **4**, corresponds well to the order of the ionic potentials of alkali metal ions. These up-field shifts are reduced by coordination of 5-fluoro-1-methyluracil in place of 1-MeUH, indicating that the electron-donating character of 1-MeU⁻ to Pd(II) is decreased by substitution with an electron-withdrawing fluoro group. These observations suggest that the up-field shifts may be rationalized in terms of π-back donation from Pd(II) *dπ*-orbital to imidato π*-orbital and the ionic potentials of alkali metals, which have also been investigated on the basis of the DFT calculation. On the basis of these characteristic features, the [M₂Pd(1-MeU)₄] complexes may be classified as a new type of metallo-podand that captures alkali metal ions.

V-F-3 Investigations of the Effects of Intramolecular Hydrogen Bonding Networks on Tripodal Trihydroxamate-Type Artificial Siderophores

MATSUMOTO, Kenji¹; OZAWA, Tomohiro¹;
JITSUKAWA, Koichiro¹; MASUDA, Hideki²
(¹Nagoya Inst. Tech.; ²IMS and Nagoya Inst. Tech.)

[*Inorg. Chem.* submitted]

The solution behavior of the iron(III) complex with tris[2-{(N-acetyl-N-hydroxy)glycylamino}ethyl]amine (TAGE) has been investigated using ¹H NMR, UV-vis, and FAB mass spectroscopies and cyclic voltammetry in efforts to characterize the hydrogen bonding networks between the amide hydrogens and coordinating aminohydroxy oxygens of the complex. Temperature dependencies of ¹H-NMR spectra for Al(III) and Ga(III) complexes of TAGE indicate that hydrogen bonding networks are maintained even in polar solvents such as DMSO-d₆ and D₂O. The UV-vis spectra of the Fe(III)-TAGE complex in various pH conditions show that TAGE forms a tris(hydroxamato)iron(III) complex in an aqueous solution from pH 4–8. On the other hand, tris[2-{(N-acetyl-N-hydroxy)propylamido}ethyl]amine (TAPE; a TAGE analogue that does not form hydrogen bonds), does not form the tris(hydroxamato)iron(III) complex in the same pH range. Both the stability constant (logβ_{FeTAGE} = 28.6; β_{FeTAGE} = [Fe^{III}TAGE]/-

($[\text{Fe}^{3+}][\text{TAGE}^{3-}]$) and pM ($-\log[\text{Fe}^{3+}]$) value for Fe^{III} -TAGE (pM 25) are comparable to those of ferrichrome, a natural siderophore ($\log\beta = 29.1$ and pM 25.2). The rate of the ligand exchange reaction between Fe^{III} -TAGE and EDTA is $6.7 \times 10^{-4} \text{ s}^{-1}$, a rate similar to those of the ferrichromes. The redox potential of Fe^{III} -TAGE in aqueous solution is -227 mV (vs. NHE) at pH 7, about 200 mV higher than those of Fe^{III} -TAPE and ferric natural trihydroxamates. The high redox potential of Fe^{III} -TAGE is interpreted in terms of the intramolecular hydrogen bonding networks wherein both iron(III) and iron(II) complexes are tightly fixed and stabilized by the TAGE ligand. In a biological activity experiment, TAGE promotes the growth of the siderophore-auxotroph gram-positive bacterium *Microbacterium flavescens*, and thus mimics the activity of ferrichrome. These results indicate that the artificial siderophore TAGE is a good structural and functional model for ferrichrome and that the intramolecular hydrogen bonding networks provide stability for the complex and allow the redox potential to increase even in an aqueous solution.

V-F-4 The Role of the Zn(II) Site in Cu,Zn SOD (1). Synthesis and Characterization of Novel Hydroperoxo-Zinc(II) Intermediates

WADA, Akira¹; JITSUKAWA, Koichiro¹; MASUDA, Hideki²

(¹Nagoya Inst. Tech.; ²IMS and Nagoya Inst. Tech.)

[*J. Amer. Chem. Soc.* Submitted]

A novel Zn–OOH species has been prepared using an original ligand bis(6-neopentylamino-2-pyridylmethyl)(2-pyridylmethyl)amine (H_2BNPA), whose synthesis was determined by ¹H-NMR and ESI-mass spectroscopic methods. The formation of $[\text{Zn}(\text{H}_2\text{BNPA})(\text{OOH})]^+$ has been confirmed from the ESI-mass spectral measurements of the reactions of $[\text{Zn}(\text{H}_2\text{BNPA})(\text{OH})]^+$ with H_2O_2 and subsequent addition of CO_2 as well as the X-ray structure of the product crystal obtained from the reaction solution kept at 0 °C under CO_2 , $[\{\text{Zn}(\text{H}_2\text{BNPA})\}_2(\text{CO}_4^{2-})]^{2+}$. Comparisons of the reactivities of Zn(II)–OOH and Cu(II)–OOH species toward CO_2 have suggested that the hydroperoxide bound to Zn(II) ion exhibits a higher nucleophilicity/basicity than that of hydroperoxide bound to Cu(II). This implies that in the 2nd half of the reaction cycle of Cu,Zn SOD, the transformation of hydroperoxide to hydrogen peroxide tends to proceed within the coordination sphere of Zn(II) site instead of within the coordination sphere of Cu(II).

V-F-5 Epoxidation Activities of Mononuclear Ruthenium-oxo Complexes with a Square Planar 6,6'-Bis(benzoylamino)-2,2'-bipyridine and Axial Ligands

JITSUKAWA, Koichiro¹; SHIOZAKI, Hiroyoshi¹; MASUDA, Hideki²

(¹Nagoya Inst. Tech.; ²IMS and Nagoya Inst. Tech.)

[*Tetrahedron Lett.* **43**, 1491 (2002)]

Some ruthenium complexes with a square planar ligand, H_2BABP , ($[\text{Ru}^{\text{II}}(\text{babp}^{2-})(\text{dmsO})_2]$ (**1**), $[\text{Ru}^{\text{II}}(\text{babp}^{2-})(\text{dmsO})(\text{im})]$ (**2**), $[\text{Ru}^{\text{II}}(\text{babp}^{2-})(\text{dmsO})(\text{py})]$ (**3**), and $[\text{Ru}^{\text{II}}(\text{babp}^{2-})(\text{dmsO})(\text{Phpy})]$ (**4**)) have been prepared as a catalyst of oxygen transfer reaction. Catalytic activity of the metal-oxo species derived by the reaction of **1** ~ **4** with PhIO has been affected by the axial ligands of the complexes, whose oxidation active species has been interpreted in terms of contribution of both characters of Ru(V)=O and Ru(IV)–O·.

V-F-6 Reactivity of Hydroperoxide Bound to a Mononuclear Non-Heme Iron Site

WADA, Akira¹; OGO, Seiji; NAGATOMO, Shigenori; KITAGAWA, Teizo; WATANABE, Yoshihito; JITSUKAWA, Koichiro²; MASUDA, Hideki¹

(¹IMS and Nagoya Inst. Tech.; ²Nagoya Inst. Tech.)

[*Inorg. Chem.* **41**, 616 (2002)]

The first isolation and spectroscopic characterization of the mononuclear hydroperoxo-iron(III) complex, $[\text{Fe}(\text{bppa})(\text{OOH})]^{2+}$ (**2**), and the stoichiometric oxidation of substrates by the mononuclear iron-oxo intermediate generated by its decomposition have been described. The purple species **2** obtained from reaction of $[\text{Fe}(\text{bppa})(\text{HCOO})](\text{ClO}_4)_2$ with H_2O_2 in acetone solution at $-50 \text{ }^\circ\text{C}$ gave characteristic UV-vis ($\lambda_{\text{max}} = 568 \text{ nm}$, $\epsilon = 1200 \text{ M}^{-1} \text{ cm}^{-1}$), ESR ($g = 7.54, 5.78$ and 4.25 , $S = 5/2$), and ESI mass spectra ($m/z = 288.5$ corresponding to the ion, $[\text{Fe}(\text{bppa})(\text{OOH})]^{2+}$), which revealed that the complex **2** is a high-spin mononuclear iron(III) complex with a hydroperoxide in an end-on fashion. The resonance Raman spectrum of **2** in d_6 -acetone revealed two intense bands at 621 and 830 cm^{-1} , in which the former band shifted to 599 cm^{-1} when reacted with ¹⁸O-labeled H_2O_2 and the latter band showed a small isotope shift to 813 and 826 cm^{-1} upon reaction with $\text{H}_2^{18}\text{O}_2$ and D_2O_2 , respectively. Reactions of the isolated (bppa)Fe^{III}–OOH (**2**) with various substrates (single turnover oxidations) exhibited that the iron-oxo intermediate generated by decomposition of complex **2** is a nucleophilic species formulated as $[(\text{bppa})\text{Fe}^{\text{III}}\text{–O}\cdot]$.

V-F-7 Reactivity Control for Epoxidation of Olefins and Dehydrogenation of Alcohols Catalyzed by Ruthenium-oxo Complexes

JITSUKAWA, Koichiro¹; MORISHIMA, Yuji¹; SHIOZAKI, Hiroyoshi¹; OKA, Yoshiyuki¹; MASUDA, Hideki²

(¹Nagoya Inst. Tech.; ²IMS and Nagoya Inst. Tech.)

[*Shokubai* **43**, 440 (2001)]

Several ruthenium complexes with tripodal polypyridine or diamidobipyridine ligands were prepared for investigation of catalytic activity on the oxygen transfer reactions. Ruthenium(V)-oxo species generated through the reaction of low-valent ruthenium complex and PhIO was observed in the ESI-mass spectroscopy. Their catalytic activities for epoxidation of olefins, hydroxy-la-

tion of alkanes and dehydrogenation of alcohols were affected by the coordination environment and redox property of the starting ruthenium complexes. These findings are explained by the hypothesis as follows: Ruthenium-oxo species generated on the complexes with non-porphine ligands show both characters of Ru(V)=O and Ru(IV)-O·. The former intermediate favors epoxidation pathway and the latter radical one.

V-F-8 Crystal Structure and Solution Behavior of the Iron(III) Complex of the Artificial Trihydroxamate Siderophore with Tris(3-aminopropyl)amine Backbone

MATSUMOTO, Kenji¹; SUZUKI, Naomi¹;
OZAWA, Tomohiro¹; JITSUKAWA, Koichiro¹;
MASUDA, Hideki²
(¹Nagoya Inst. Tech.; ²IMS and Nagoya Inst. Tech.)

[*Eur. J. Inorg. Chem.* **10**, 2481 (2001)]

Microorganisms produce low molecular weight compounds called siderophores for an uptake of iron. A large number of siderophores have hydroxamates or catecholates as the iron binding site that exhibits very high affinity for iron(III) ion, and their siderophores form very stable iron(III) complexes. The high stability of Fe(III)-siderophore complexes is attributed to not only such chelating effect but also hydrogen bonding and van der Waals interactions and predisposition of ligands. Thus, the ligand backbones are quite important for the stabilization of iron(III) complexes. Many tripodal artificial siderophores were synthesized as ferrichrome and enterobactin analogues; the synthetic siderophores adopt various tripodal backbones as follows, *e.g.*, tris(2-aminoethyl)amine (TREN), triaminomethylbenzene, 1,5,9-triazacyclododecane, nitrilotriacetic acid, 1,1,1-tris{(2-carboxyethoxy)methyl}propane. Among such tripodal backbones, TREN has been frequently used. Recently, we also have reported the synthesis of tris[2-((N-acetyl-N-hydroxy)glycylamino)ethyl]amine (TAGE) as the artificial siderophore with TREN anchor, whose iron(III) complex showed extremely high stability ($\log\beta = 28.7$). From the crystal structure of the iron(III) complex, this higher stability was revealed to be attributed to the intramolecular hydrogen bonding networks. However, the tripodal anchors such as TREN have been reported to make reduce the stability of iron(III) complexes than the natural siderophore-iron (III) complexes, which are presumed to be due to the small size of the anchor for an iron(III) chelation. On the other hand, tris(3-aminopropyl)amine (TRPN), whose alkyl chains are one methylene longer than TREN, has not been much used, and the details are little described, despite the similarity in these structures. At this stage, we newly synthesized tris[3-(N-acetyl-N-hydroxy)glycylamino]propylamine (TAGP, Figure 1) as a trihydroxamate artificial siderophore with TRPN anchor in order to examine the efficiency of the size. Tris[3-(N-acetyl-N-hydroxy)glycylamino]propylamine (TAGP) forms the 1 : 1 tris(hydroxamato)-iron(III) complex even at a low pH (~2), which promotes the growth of the siderophore-auxotrophic mutant *Microbacterium flavescens*. Here,

we described the crystal structure and solution behavior of its iron(III) complex.

V-F-9 Reverse Reactivity in Hydroxylation of Adamantane and Epoxidation of Cyclohexene Catalyzed by the Mononuclear Ruthenium-oxo Complexes with 6-Substituted Tripodal Polypyridine Ligands

JITSUKAWA, Koichiro¹; OKA, Yoshiyuki¹;
EINAGA, Hisahiko¹; MASUDA, Hideki²
(¹Nagoya Inst. Tech.; ²IMS and Nagoya Inst. Tech.)

[*Tetrahedron Lett.* **42**, 3467 (2001)]

The electronic character of the ruthenium complexes with tripodal polypyridine ligands, which is controlled by the substituted groups at pyridine 6-position, gives rise to differences in the reactivity for the ruthenium catalyzed hydroxylation of adamantane and epoxidation of cyclohexene with PhIO as an oxidant; Ru complexes containing electron-withdrawing groups promote the epoxidation, while those containing electron-donating groups promote the hydroxylation.

V-F-10 Characterization of an NH- π Interaction in Co(III) Ternary Complexes with Aromatic Amino Acids

KUMITA, Hideyuki¹; KATO, Takashi¹;
JITSUKAWA, Koichiro¹; EINAGA, Hisahiko¹;
MASUDA, Hideki²
(¹Nagoya Inst. Tech.; ²IMS and Nagoya Inst. Tech.)

[*Inorg. Chem.* **40**, 3936 (2001)]

The NH- π interaction has been detected in the crystal structures of Co(III) ternary complexes with N,N-bis(carboxymethyl)-(S)-phenylalanine (BCMPA) and aromatic amino acids including: (S)-phenylalanine ((S)-Phe), (R)-phenylalanine ((R)-Phe), and (S)-tryptophan ((S)-Trp)). Additionally, this interaction has been studied in solution for Co(III) ternary complexes with BCMPA or NTA (NTA = nitrilotriacetic acid) and several amino acids (AA) by means of electronic absorption, circular dichroism (CD), and ¹H NMR spectroscopies. The CD intensities of the Co(III) complexes with aromatic amino acids measured in the *d-d* region ($\sim 20.5 \times 10^3 \text{ cm}^{-1}$) are significantly decreased in ethanol solutions relative to water. Analogous complexes with aliphatic amino acids do not exhibit this solvent effect. The ¹H NMR spectra of the Co(III) complexes with aromatic amino acids measured in DMSO-d₆ and D₂O exhibit up-field shifts of the N-H peaks compared with those with aliphatic amino acids for both cases, which suggest a shielding effect due to the aromaticity. The up-shift values coincide with those experimentally evaluated from the crystal structures. The magnitude of the upfield shifts observed in DMSO-d₆ agrees well with Hammett's rule and similar tendency is slightly characterized also in D₂O, indicating that the increase of π -electron densities on the aromatic rings exerts a larger shielding effect for the NH protons and it is reduced in aqueous solution. In ligand-substitution reactions of the

carbonatocobalt(III) complexes with amino acids, the yields of those with aromatic amino acids are higher than the yields obtained for complexes with aliphatic amino acids. This observation is discussed in connection with the important contribution of the NH- π interaction as one of the promotion factors in the reaction.

V-F-11 The Role of the Zn(II) Site in Cu,Zn SOD. (2) Evidence of Superoxide Disproportionation Catalyzed by Sterically- and Electrostatically-Controlled Zinc(II) Complexes

WADA, Akira¹; JITSUKAWA, Koichiro¹; MASUDA, Hideki²

(¹Nagoya Inst. Tech.; ²IMS and Nagoya Inst. Tech.)

[J. Amer. Chem. Soc. submitted]

The role of the Zn(II) site in the disproportionation reaction of superoxide catalyzed by Cu,Zn superoxide dismutase (Cu,Zn SOD) has been systematically examined using sterically- and electrostatically-controlled Zn(II) complexes in an aprotic solvent (MeCN/DMSO (9:1)) by cyclic voltammetry, ESI-mass spectroscopy and ESR spectroscopy. Interestingly, higher SOD activity was observed in the Zn(II) complexes with lower Lewis acidity and in Zn(II) complexes without a superoxide-accessible site. These findings clearly indicate that the efficient catalytic SOD reaction is due to efficient access of superoxide to the Zn(II) ion. Here we offer a new proposal for the role of Zn(II) site in Cu, Zn SOD and propose an alternate mechanism for the 2nd step of SOD reaction.

V-F-12 SOD Activities of the Copper Complexes with Tripodal Polypyridylamine Ligands Having a Hydrogen Bonding Site

JITSUKAWA, Koichiro¹; HARATA, Manabu¹; ARII, Hidekazu¹; SAKURAI, Hiromu²; EINAGA, Hisahiko¹; MASUDA, Hideki³

(¹Nagoya Inst. Tech.; ²Kyoto Pharmaceutical Univ.; ³IMS and Nagoya Inst. Tech.)

[Inorg. Chim. Acta **324**, 108 (2001)]

For investigation of the correlation with the coordination structures of the copper complexes and their superoxide dismutation activities, four mononuclear copper complexes with tris(2-pyridylmethyl)-amine derivatives containing pivalamido or neopentyl-amino groups at pyridine 6-position, [Cu(tnpa)(OH)]ClO₄ (**1**), [Cu(tapa)Cl]ClO₄ (**2**), [Cu(tapa)(OH)]ClO₄ (**3**), and [Cu(bppa)](ClO₄)₂ (**4**), and two dinuclear copper complexes, [Cu₂(tppen)(H₂O)₂](ClO₄)₂ (**5**) and [Cu₂(tppen)Cl₄] (**6**), were prepared as single crystals suitable for X-ray analysis except the complex **3**. Such hydrogen bonding moiety at pyridine 6-position of these ligands is regarded as a Arg 141 residue around copper site in native bovine superoxide dismutase (SOD). Coordination geometry around copper ion in **1** ~ **3**, **5**, and **6** was determined to have 5-coordinate trigonal bipyramidal or square pyramidal structure both in crystal and solution phases on the basis of their X-ray

analyses or spectroscopic results. However, that in **4** was 4-coordinate square planar structure. The redox potentials of the mononuclear complexes, **1** ~ **4**, (Cu(II)/Cu(I) couple) were within the range between -330 mV (vs. NHE at pH 7. O₂/O₂⁻) and + 890 mV (vs. NHE. O₂⁻/H₂O₂), which were in good range for superoxide dismutation, so that these complexes were used for investigating their catalytic activity. Moderate dismutation activities were demonstrated in the cases of **1** ~ **3** in comparison with other mononuclear copper complexes previously reported, although **4** showed the lowest activity of all. The distorted structure around copper center, such as 5-coordinate trigonal bipyramidal or square pyramidal structure, is important for demonstrating SOD activity. In addition, the activities caused by the dinuclear complex, **5** and **6**, were higher than those by the mononuclear ones. 6-Neopentylamino or 6-amino group of the tripodal polypyridine ligands, which is designed as a hydrogen bonding moiety, plays an important role for acceleration of activity in the SOD mimics through stabilization of superoxide species binding to the metal center.

V-F-13 Site-Selective Recognition of Amino Acids by Co(III) Complexes Containing a (N)(O)₃-Type Tripodal Tetradentate Ligand

KUMITA, Hideyuki¹; MORIOKA, Taiju¹; OZAWA, Tomohiro¹; JITSUKAWA, Koichiro¹; EINAGA, Hisahiko¹; MASUDA, Hideki²

(¹Nagoya Inst. Tech.; ²IMS and Nagoya Inst. Tech.)

[Bull. Chem. Soc. Jpn. **74**, 1035 (2001)]

The bis-*N,N*-carboxymethyl-(*S*)-phenylalaninato carbonato cobalt(III) complex, [Co(bcmpa)(CO₃)]²⁻, has been prepared as a simple model that enables the recognition of an amino acid (Haa) whose coordination behaviours in solution have been characterized by electronic absorption (AB), circular dichroism (CD) and ¹H-NMR spectroscopies. The reaction of the K₂[Co-(bcmpa)(CO₃)] complex with amino acids (Haa) has predominantly afforded the [Co(bcmpa)(aa)] complex in the *trans*(*N*)-configuration mode, rather than in the *cis*(*N*)-form. By using amino acid derivatives with bulky substituents at their amino or carboxylate sites under a neutral condition, the reactions have been demonstrated to be initiated by coordination of the amino nitrogen site. Interestingly, the *cis*(*N*)-complex, which is isolated as a minor product, isomerizes to the *trans*(*N*)-form in the presence of active charcoal under pH 7 in an aqueous solution. The site-selective coordination of Haa to the [Co(bcmpa)(CO₃)]²⁻ complex and the stereoselective isomerization of the [Co(bcmpa)(aa)]⁻ complex have been explained to be regulated by weak non-covalent interactions within the ligands, whose origin has been discussed based on a detailed examination of the crystal structures of the *trans*(*N*)- and *cis*(*N*)-K[Co(bcmpa)(aa)] complexes.

V-G Probing Time-Dependent Processes in Solution with Time-Resolved Spectroscopic Methods

A solute molecule surrounded by solvent molecules is exposed to dynamic environments of rapidly changing energy, polarity, or relative distance and orientation with adjacent molecules. The effects of these fluctuations, which are caused by the room temperature solvent molecules, are clearly demonstrated when the solute molecule experiences a chemical reaction. Intermolecular energy transfer and rotational or translational diffusion determine the fate of the chemical reaction.

Time-resolved spectroscopy is quite effective for studying time-dependent events occurring in solution. We use various types of time-resolved spectroscopy for observing dynamical processes. In this Annual Review, we report on five research projects, in which we use femtosecond time-resolved fluorescence spectroscopy with single channel detection, picosecond time-resolved fluorescence spectroscopy with multi-channel detection, picosecond time-resolved Raman spectroscopy, and nanosecond time-resolved infrared spectroscopy. We discuss (i) fast internal conversion of biphenyl, (ii) disagreement between Stokes- and anti-Stokes scattering frequencies observed under strong pump or probe light field, (iii) photoinduced Cl transfer reaction between biphenyl and carbon tetrachloride that results in the generation of the trichloromethyl (CCl_3) radical, (iv) solvent- and temperature-dependent Raman spectral changes of S_1 *trans*-stilbene and the mechanism of the *trans* to *cis* isomerization, and (v) picosecond dynamics of stepwise double proton-transfer reaction in the excited state of the 2-aminopyridine/acetic acid system.

V-G-1 Femtosecond Time-Resolved Anisotropy Measurement of Biphenyl Fluorescence

IWATA, Koichi¹; TAKEUCHI, Satoshi; TAHARA, Tahei²

(¹IMS and Univ. Tokyo; ²IMS and RIKEN)

The fluorescence intensity and its anisotropy decay of biphenyl were observed in the hexane solution. Biphenyl in hexane was photoexcited with a linearly polarized femtosecond light pulse at 260 nm. Time dependence of the fluorescence intensity as well as its anisotropy was measured with the up-conversion method. The observed fluorescence decay curve showed a fast decay component of 0.4 ps, in addition to a slow component that corresponds to the reported fluorescence decay time of 16 ns. The fluorescence anisotropy was approximately 0.4 at time 0, indicating that the direction of the fluorescence transition dipole at time 0 is same as the S_2 - S_0 absorption transition at 270 nm. The observed decay curve of the anisotropy was well fitted by a superposition of two exponential decay functions, with the time constants of 0.3 ps and 9 ps. The S_2 - S_1 internal conversion rate of biphenyl is thus estimated to be 0.3 ps.

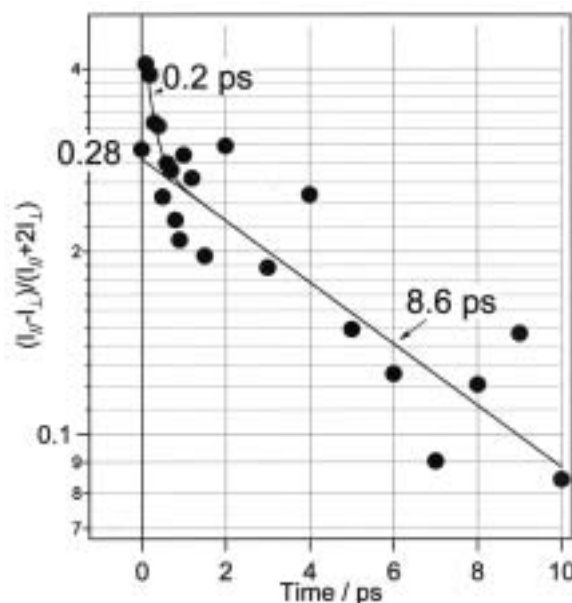


Figure 1. Observed curve of fluorescence anisotropy decay of biphenyl in hexane.

V-G-2 Effect of Pump and Probe Light Field on Picosecond Time-Resolved Resonance Raman Spectra of S_1 *trans*-Stilbene. Disagreement between Stokes- and Anti-Stokes Scattering Frequencies

IWATA, Koichi

(IMS and Univ. Tokyo)

[Bull. Chem. Soc. Jpn. 75, 1075 (2002)]

Picosecond time-resolved spontaneous resonance Raman spectra of the first excited singlet (S_1) state of *trans*-stilbene were measured with various power densities of pump or probe light, for both the Stokes and anti-Stokes scattering regions. Careful calibration of the peak positions of the 285 cm^{-1} Raman bands reveals that the Stokes scattering band and the anti-Stokes

scattering band shift to the same direction in absolute wavenumber, or to the opposite directions in Raman shift, when the pump or probe power density is increased. The direction of the wavenumber shift caused by the pump light field is opposite to that caused by the probe. Because of these apparent peak shifts, the Stokes Raman band and the anti-Stokes Raman band are recorded at different Raman shifts. The intrinsic change of the vibrational level spacing and the apparent peak shift caused by the pump or probe light field can be clearly separated by calculating the "symmetric" and "anti-symmetric" components from the Stokes and anti-Stokes peak positions. The experimental results are not explained by the optical Stark effect in its simplest form. Possible mechanisms to account for the results are discussed.

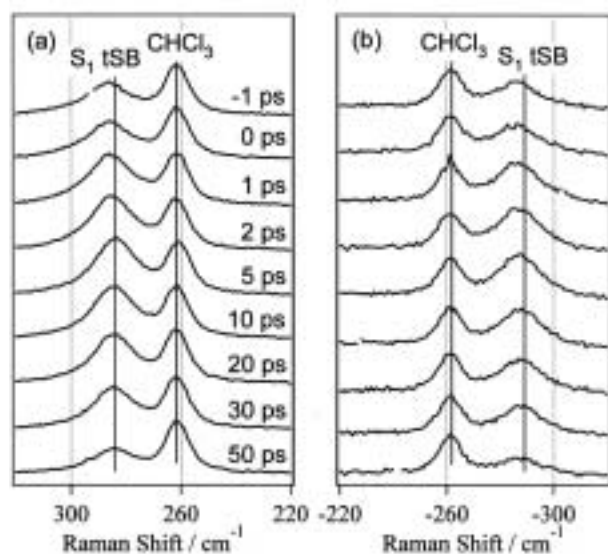


Figure 1. Time-resolved Raman spectra of S_1 *trans*-stilbene in chloroform. Stokes scattering bands (a) and Anti-Stokes scattering bands (b). Raman bands from S_1 *trans*-stilbene and solvent chloroform as well as time delay for each spectrum is indicated in the figure.

V-G-3 Photoinduced Cl Transfer Reaction between Biphenyl and Carbon Tetrachloride Studied by Nanosecond Time-Resolved Infrared Spectroscopy and Picosecond Time-Resolved Fluorescence Spectroscopy

IWATA, Koichi¹; TAKAHASHI, Hiroaki²
(¹IMS and Univ. Tokyo; ²Waseda Univ.)

[*J. Mol. Struct.* **598**, 97 (2001)]

Photochemical reaction between biphenyl and carbon tetrachloride is studied with nanosecond time-resolved infrared spectroscopy and picosecond time-resolved fluorescence spectroscopy. Fluorescence lifetime of biphenyl in carbon tetrachloride solutions is measured with a picosecond time-resolved fluorescence spectrometer. The recorded lifetime is 3.8 ps, shorter than fluorescence lifetime in cyclohexane by a factor of four thousands. After the photoexcitation of biphenyl in carbon tetrachloride, the trichloromethyl (CCl_3) radical is formed as a reaction intermediate, which is confirmed

by the detection of the radical's 896 cm^{-1} infrared band with nanosecond time-resolved infrared spectroscopy. One of the Cl atoms in solvent carbon tetrachloride is transferred to biphenyl to form the CCl_3 radical and a biphenyl-Cl adduct. Together with the already reported spectroscopic detection of the CCl_3 radical as an intermediate in photochemical reactions of *trans*-stilbene or anthracene with carbon tetrachloride, it is likely that this series of reactions are common for aromatic molecules.

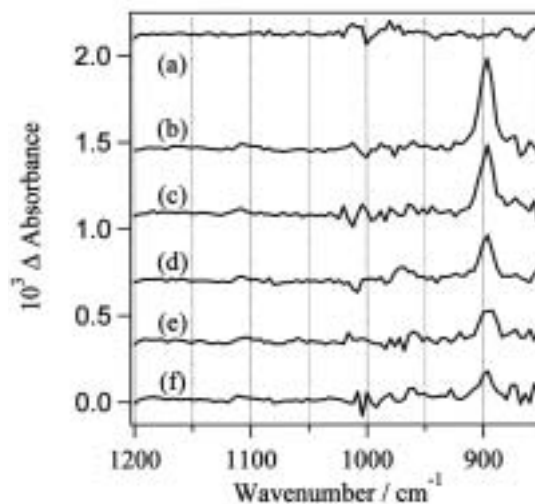


Figure 1. Time-resolved infrared difference spectra of biphenyl after photoexcitation in a carbon tetrachloride solution. Averaged spectrum for (a) -5 to $0\ \mu\text{s}$, (b) 0 to $5\ \mu\text{s}$, (c) 10 to $15\ \mu\text{s}$, (d) 20 to $25\ \mu\text{s}$, (e) 30 to $35\ \mu\text{s}$, and (f) 40 to $45\ \mu\text{s}$. Transient absorption band from the trichloromethyl (CCl_3) radical is observed at 896 cm^{-1} .

V-G-4 Analysis of the Solvent- and Temperature-Dependent Raman Spectral Changes of S_1 *trans*-Stilbene and the Mechanism of the *Trans* to *Cis* Isomerization: Dynamic Polarization Model of Vibrational Dephasing and the C=C Double-Bond Rotation

IWATA, Koichi¹; OZAWA, Ryosuke²;
HAMAGUCHI, Hiro-o²
(¹IMS and Univ. Tokyo; ²Univ. Tokyo)

[*J. Phys. Chem. A* **106**, 3614 (2002)]

Solvent- and temperature-dependent band shape changes of the olefinic C=C stretch Raman band of S_1 *trans*-stilbene have been analyzed on the basis of the dynamic polarization model. The analysis has shown that the solvent-induced dynamic polarization gives rise to the dephasing of the C=C stretch vibration and, concomitantly, triggers and facilitates the rotation around the C=C bond leading to the *trans* to *perpendicular* (and eventually to *cis*) isomerization. Picosecond time-resolved Raman spectra have been measured in three alkane solvents, hexane, octane, and decane at a number of different temperatures ranging from 268 K to 338 K and a total of 40 peak positions and the bandwidths have been determined for the C=C stretch band. The correlation plot of the bandwidth against peak position shows a clear linear relationship that is predicted by the dynamic polarization model.

Picosecond time-resolved fluorescence measurements have been performed in the same three alkane solvents at five different temperatures from 283 K to 313 K and 15 rates of the *trans* to *perpendicular* isomerization have been determined. The plot of the peak position against the rate of isomerization indicates another linear relationship between these two quantities which have no obvious reason to be correlated with each other. The dynamic polarization model accounts very well for this linear relationship and yields a new formula that relates the rate of isomerization to the frequency of the solvent-induced dynamic polarization. This formula seems to possess certain generality because it shows an excellent numerical agreement with the Arrhenius formula. The new formula derived from the dynamic polarization model gives the molecular-level details of the reaction process as to how the reaction is triggered and in what time scale the reaction actually proceeds. A new view of the photoisomerization of *trans*-stilbene has thus been obtained.

V-G-5 Picosecond Dynamics of Stepwise Double Proton-Transfer Reaction in the Excited State of the 2-Aminopyridine/Acetic Acid System

**ISHIKAWA, Hironori²; IWATA, Koichi¹;
HAMAGUCHI, Hiro-o²**
(¹IMS and Univ. Tokyo; ²Univ. Tokyo)

[*J. Phys. Chem. A* **106**, 2305 (2002)]

The dynamics of the amino-imino double proton-transfer tautomerism reaction of the 2-aminopyridine (2AP)/acetic acid system in hexane have been investigated with steady-state absorption, steady-state fluorescence, and picosecond time-resolved fluorescence spectroscopies. It has been confirmed that the double proton transfer reaction takes place in the excited state of the double hydrogen-bonded complex of 2AP with acetic acid. The imino tautomer fluorescence shows a rise behavior with a 5 ps time constant at 480 nm, while a decay with a 5 ps time constant has been observed at 360 nm. The rate of this kinetics is reduced to 7 ps with deuterium substitution. From the comparison with the steady-state fluorescence spectra of proton-transferred model compounds, the 5 ps decaying species has been identified as the intermediate in which one proton is transferred from acetic acid to 2AP. It is thus concluded that the 5 ps time constant represents the second proton-transfer process which follows the first proton transfer that is too fast to be detected in the present experiment. The photoexcited double hydrogen-bonded complex of 2AP and acetic acid undergoes a stepwise double proton-transfer reaction within 5 ps in the excited state.

V-H Structures and Properties of Lanthanoid-Metallofullerenes

Lanthanoid-containing metallofullerenes with C_{82} cages, $M@C_{82}$ (M is a lanthanoid metal atom), are the most widely investigated metallofullerenes. Accordingly to the oxidation state of the metal atom inside, they are classified into two groups; in one the metal atom takes the divalent state, and in the other it takes the trivalent state. Whether the two types of metallofullerenes have a common cage have been one of questions of lanthanoid-metallofullerenes. Recently we revealed that two types of metallofullerenes have a common cage and investigated the correlation between the absorption spectra and the cage structures on lanthanoid-metallofullerenes.

V-H-1 Spectroscopic Studies of Endohedral Metallofullerenes

KODAMA, Takeshi¹; KUSUDA, Masaya¹; OZAWA, Norio¹; FUJII, Ryosuke¹; SAKAGUCHI, Koichi¹; NISHIKAWA, Hiroyuki¹; IKEMOTO, Isao¹; KIKUCHI, Koichi²; MIYAKE, Yoko¹; ACHIBA, Yohji¹

(¹Tokyo Metropolitan Univ.; ²IMS and Tokyo Metropolitan Univ.)

[*New diamond and Frontier Carbon Technology* **11**, 367 (2001)]

We have measured the absorption spectra of the cations of $La@C_{82}$ and $Ce@C_{82}$, which are trivalent-type metallofullerenes. The obtained spectra resemble not only each other but also those of the neutral species of $Ca@C_{82}(IV)$ and $Tm@C_{82}(III)$, which are divalent-type metallofullerenes. Moreover we found that four metallofullerenes have an identical cage. To assign the absorption spectra, we performed a semi-empirical calculation at the level of single configuration interaction for $Ca@C_{82}(IV)$. It was revealed that any charge

transfer transitions from the C_{82} cage to the encapsulated metal atom cannot have large oscillator strength.

V-H-2 Structural Study of Three Isomers of $Tm@C_{82}$ by ¹³C NMR Spectroscopy

KODAMA, Takeshi¹; OZAWA, Norio¹; MIYAKE, Yoko¹; SAKAGUCHI, Koichi¹; NISHIKAWA, Hiroyuki¹; IKEMOTO, Isao¹; KIKUCHI, Koichi²; ACHIBA, Yohji¹

(¹Tokyo Metropolitan Univ.; ²IMS and Tokyo Metropolitan Univ.)

[*J. Am. Chem. Soc.* **124**, 1452 (2002)]

The ¹³C NMR spectra were measured for three isomers of $Tm@C_{82}$, which is one of the divalent metallofullerenes. The molecular symmetries were determined for each isomer: isomer I has C_s symmetry, isomer II has C_2 symmetry, and isomer III has C_{2v} symmetry. Moreover the cage structure of $Tm@C_{82}(III)$ was found to be $C_{82}(9)$. As a result, it was revealed that $Tm@C_{82}(III)$ has a cage identical to that of $La@C_{82}$, which is one of the trivalent metallofullerenes.

V-I Development of Organic Superconductors

Since the discovery of superconductivity in a series of salts of TMTSF, TCF (tetrachalcogenafulvalene) derivatives have served as π -electron donors for the development of new organic superconductors. Although considerable research effort in this field has focused on the construction of TCF-type donors with extended π -conjugation, these donors, except for the DTEDT donor, failed to yield any organic superconductors. Besides TCF derivatives, our reported BDA-TTP donor gives three superconducting salts, but its π -electron system is the as that of TCF derivatives. Then it is possible that donor molecules with a less extended π -system that that of TCF derivatives produce superconductor? We attempted to find an answer to this question in the DHTTF donor system. We have also investigated the properties other salts of BDA-TTP.

V-I-1 New Organic Superconductors Consisting of an Unprecedented π -Electron Donor

NISHIKAWA, Hiroyuki¹; MORIMOTO, Takanobu¹; KODAMA, Takeshi¹; IKEMOTO, Isao¹; KIKUCHI, Koichi²; YAMADA, Jun-ichi³; YOSHINO, Harukazu⁴; MURATA, Keizo⁴

(¹Tokyo Metropolitan Univ.; ²IMS and Tokyo Metropolitan Univ.; ³Himeji Inst. Tech.; ⁴Osaka City

Univ.)

[*J. Am. Chem. Soc.* **124**, 730 (2002)]

We designed and synthesized the DODHT donor with a reduced π -system as well as a bulky cis-fused dioxane ring. This donor forms crystalline salts with AsF_6 and PF_6 that display a variety of the pressure-induced resistive behavior and become superconducting at 3.3 and 3.1 K under 16.5 kbar pressure. X-ray analy-

sis show the donor molecules stacked head-to-tail to form the β'' -type arrangement with weak intermolecular interactions in both salts.

V-I-2 Tetrachloroferrate (III) Salts of BDH-TTP and BDA-TTP: Crystal Structures and Physical Properties

KIKUCHI, Koichi¹; NISHIKAWA, Hiroyuki²; IKEMOTO, Isao²; TOITA, Takashi³; AKUTSU, Hiroki³; NAKATSUJI, Shin-ichi³; YAMADA, Jun-ichi³

(¹IMS and Tokyo Metropolitan Univ.; ²Tokyo Metropolitan Univ.; ³Himeji Inst. Tech.)

[*J. Solid State Chem.* in press]

Three FeCl_4 salts based on non-TTF donors, BDH-TTP and BDA-TTP, have been prepared and characterized as κ -(BDH-TTP)₂FeCl₄, β -(BDA-TTP)₂FeCl₄, and (BDA-TTP)₃FeCl₄·PhCl. The κ -(BDH-TTP)₂FeCl₄ salt, with a room-temperature conductivity (σ_{rt}) of 39 Scm^{-1} , is metallic down to 1.5 K, and its magnetic susceptibility obeys the Curie-Weiss law with a Curie constant (C) of 4.25 emuKmol^{-1} and a Weiss constant (θ) of 0.041 K. β -(BDA-TTP)₂FeCl₄ exhibits metallic behavior ($\sigma_{\text{rt}} = 9.4 \text{ Scm}^{-1}$) with a sharp metal-to-insulator (MI) transition ($T_{\text{MI}} = 113 \text{ K}$) and antiferromagnetic ordering with the Néel temperature of near 8.5 K, whereas the solvated (BDA-TTP)₃FeCl₄·PhCl salt is a semiconductor with a thermal activation energy of 0.11 eV ($\sigma_{\text{rt}} = 2.0 \times 10^{-2} \text{ Scm}^{-1}$) and exhibits Curie-Weiss behavior ($C = 4.42 \text{ emuK mol}^{-1}$, $\theta = -0.35 \text{ K}$).

V-J Stereodynamics of Crossed Beam Reactions

Reactions of metastable noble gas atoms with small molecules have provided a long-standing interest because of the diversity of reaction channels. Penning ionization consists of a spontaneous ionization of intermediate collisional complex, therefore it is a process of fundamental interest behind its importance in plasma and astrochemistry. It has been demonstrated that Penning ionization probes the electron density distribution of the orbital from where the electron is removed, and the collision energy dependence of the ionization cross section has been suggested to be a good measure to clarify anisotropy of intermolecular forces. The reactivity depends not only on the anisotropy of the coupling matrix but also on stereo-anisotropic intermolecular forces. Therefore we study how such steric effect depends on collision energy, as well as on mutual orientation of reactants.

V-J-1 Stereo-Selectivity in the Penning Ionization Reaction of CH_3X ($\text{X} = \text{Cl}, \text{Br}, \text{I}$) + $\text{Ar}({}^3\text{P}) \rightarrow \text{CH}_3\text{X}^+ + \text{Ar} + \text{e}^-$

OKADA, Seiki¹; OHOYAMA, Hiroshi¹; KASAI, Toshio²
(¹Osaka Univ.; ²IMS and Osaka Univ.)

[*Chem. Phys. Lett.* **355**, 77 (2002)]

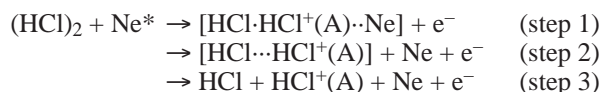
Recently, we have performed the direct observation of steric effect in CH_3Cl Penning ionization with the metastable argon atom using the hexapole state-selector, and we verified a good correlation between stereo-selectivity in the Penning ionization cross section and the spatial distribution of the electron density of HOMO orbital of the CH_3Cl molecule. In order to substantiate the above-mentioned relationship, we extended the study by replacing halogen atom of the molecule. In the present study, we determined the steric opacity functions for the two similar Penning ionization reactions of CH_3X ($\text{X} = \text{Br}, \text{I}$) + $\text{Ar}({}^3\text{P}) \rightarrow \text{CH}_3\text{X}^+ + \text{Ar} + \text{e}^-$ at an average collision energy of 0.1 eV. We find that the most reactive site shifts from the collinear X-end toward sideways as the mass number of X increases (i.e. from Br to I). Taking into account the previously obtained result for the CH_3Cl reaction, a good correlation can be seen again between the steric opacity function and the electron density distributions of the lone-pair HOMO orbital of CH_3X molecule.

V-J-2 Evidence for the $\text{HCl}^+(\text{A})$ Formation in the Reaction of $\text{Ne}({}^3\text{P})$ with the Size-Selected HCl Dimer Using an Electrostatic Hexapole Field

IMURA, Kohei; OHOYAMA, Hiroshi²; KASAI, Toshio¹
(¹IMS and Osaka Univ.; ²Osaka Univ.)

[*Chem. Lett.* 1136 (2001)]

There has been no evidence so far that reaction of $\text{Ne}({}^3\text{P})$, with the HCl dimer produces $\text{HCl}^+(\text{A})$, though the corresponding HCl monomer reaction produces $\text{HCl}^+(\text{A})$ in the vibrational states $\nu' = 0, 1$, and 2. Naaman and co-workers pointed out that chemical reactivity of monomers and clusters strongly depends on species of the reactant atom. For the $\text{Ne}^+(\text{HCl})_2$ reaction, there are many exit channels open such as electronic excitation, ionization, and dissociation from energetic point of view. In this work, Penning ionization of $\text{Ne}({}^3\text{P})$ metastable atom with size-selected HCl dimer was studied by using an electrostatic hexapole state-selector and chemiluminescence detection. We find that the HCl dimer can also produce $\text{HCl}^+(\text{A})$ ions in the reaction with $\text{Ne}({}^3\text{P})$ just like its corresponding monomer reaction. The internal energy distribution of $\text{HCl}^+(\text{A})$ in the dimer reaction is found to be cooler than that in the monomer reaction, reflecting the third-body effect in the dimer. The suggested reaction scheme is shown as follows.



V-K Photodissociation Dynamics

Photo-initiated reaction of weakly hydrogen bonded halide dimer, $(\text{HX})_2$, has a basic potentiality to produce $[\text{XHX}]$ transient specie by means of the hydrogen atom elimination from $(\text{HX})_2$ dimer. By measuring translational energy distribution of the eliminated hydrogen atom, one can extract information about van der Waals interaction of reactants in the $\text{X} + \text{HX}$ reaction system. We study the 243-nm photo-dissociation of the DCl clusters by using a Doppler-selected TOF (DS-TOF) technique in order to detect $[\text{CIDCl}]$ transient species. We employed the hexapole method to select only the DCl dimer in cluster beam and to exclude any ambiguity about precursor cluster size.

V-K-1 Photodissociation of DCI Dimer Selected by an Electrostatic Hexapole Field Combined with Doppler-Selected TOF Technique: Observation of [CIDCI] Transient Species

CHE, Dock-Chil; HASHINOKUCHI, Mitihiro¹; SHIMIZU, Yuichiro; KASAI, Toshio¹
(¹IMS and Osaka Univ.)

[*Phys. Chem. Chem. Phys.* **3**, 4979 (2001)]

The photodissociation of DCI dimer, which is preferentially selected from the cluster beam using a hexapole electrostatic field prior to the photolysis, has been studied by a Doppler-selected time-of-flight (DS-TOF) technique at 243 nm. We observed the [CIDCI] transient species through the hydrogen atom elimination from (DCI)₂. By measuring the dependence of the enhancement for the photodissociated D-atom signal upon the hexapole voltage, we find that the DS-TOF spectrum exhibits two kinds of velocity components; one is fast velocity component which originates from only dimer photodissociation, and the other is slow velocity component which originates from not only dimer but also higher sizes of the DCI clusters. For the fast velocity component, the observed spectrum shows an oscillating structure, which could reflect a footprint of nascent internal states (mainly vibration) of the [CIDCI] transient species. The spacing of the observed peaks is about 1000 cm⁻¹, which is much smaller than

that of the normal stretching frequency (2091 cm⁻¹) of the DCI monomer. This result suggests that the observed spectrum reflects the strong perturbation from the Cl atom in [CIDCI].

V-K-2 A New Channel of Hydrogen Elimination in the 121.6-nm Photodissociation of Formic Acid Detected by a Doppler-Selected TOF Mass Spectrometry

HASHINOKUCHI, Mitihiro¹; KOUMURA, Ryouji²; CHE, Dock-Chil; KASAI, Toshio¹
(¹IMS and Osaka Univ.; ²Osaka Univ.)

[*J. Mass Spectrom. Soc. Jpn.* **50**, 7 (2002)]

The 121.6-nm photodissociation of formic acid was investigated by a Doppler-Selected TOF mass spectrometry (DS-TOF-MS) that enables us to map out 3D velocity distributions of photodissociated products through REMPI for the H atoms. The main channel is found to be the HCOO* formation. A new channel of H + CO + OH(X) hydrogen elimination reaction is observed. We estimate that the branching ratio to [H + HCOO*] with respect to [H + CO + OH(X)] is ~ 5 and those to HCOO(X), HOCO(X) and [2H + CO₂] formation channels are very small. These results show that the DS-TOF-MS method is useful to determine branching ratios and internal energy distributions of photodissociated products in both excited and ground states.

V-L Non-Destructive Structure Determination of Neural Clusters

Van der Waals clusters give a great interest as interfaces on chemical and physical properties between the gas phase and the condensed phase. Especially, the relationship between structure and dynamics is often called stereodynamics. From this sense, it is important to determine structure of cluster and to select special size and/or geometric isomers of cluster. In general, relative population of geometric isomers has been discussed in terms of stability of the isomers at equilibrium structure, but such a common sense is not necessarily appropriate in the case if dynamics of the cooling process induces special selectivity on isomer formation. It is plausible that different conditions for cluster beam preparation produced different clusters. Along this context, we investigate cooling process of geometric isomers during cluster formation.

V-L-1 Focusing and Selecting the Linear Type HBr-N₂O by Using a 2 m Long Electrostatic Hexapole Field

OKANO, Akihiko¹; OHYAMA, Hiroshi¹; KASAI, Toshio²
(¹Osaka Univ.; ²IMS and Osaka Univ.)

[*J. Chem. Phys.* **116**, 1325 (2002)]

Although N₂O-HCl and N₂O-HBr are expected to have similar two types of geometric isomers from the analogs of ONN-HF, it has been reported that extensive searches revealed only bent N₂O-HCl and N₂O-HBr and that there was no trace of linear ONN-HCl or

ONN-HBr. We performed focusing and selecting the HBr-N₂O cluster beam by using a 2m-long electrostatic hexapole field. The observed focusing curve shows a clear evidence that the linear type HBr-N₂O isomer which has symmetry of symmetric top molecule was preferentially produced in the cluster beam nevertheless our previous *ab initio* calculation predicts the bent type isomer. The best fit simulation for the experimental focusing curve was achieved only if we assume vibrational excitation in the van der Waals mode of the linear type HBr-N₂O. The permanent dipole moment is determined to be 0.70 ± 0.05 D. The potential energy of the O-end bent type is more stable than the N-end linear type. From the potential energy surface made by transferring HBr-N₂O geometry, the formation of the

two isomers is selected at a fairly long bond length between HBr and N₂O.

V-M Reaction Dynamics at Surfaces

The interaction of hydrogen with surfaces has been a subject of intense interest in surface science because it is the simplest paradigm relevant to single valence electron. The reaction of hydrogen on a surface can be an ideal candidate for testing validity of various concepts in surface chemical reaction. Also, it is known that adsorbed hydrogen can provide a significant effect on kinematical and electronic properties in the surface region of materials, inducing embrittlement and fracture. To understand how hydrogen interacts with surface atoms and reacts with other atoms on the surface and its possible diffusion into and from the bulk is important in various fields; heterogeneous catalysis, material science, metallurgy, hydrogen storage, etc. These phenomena embodied in hydrogen interaction with metal surfaces encompass most of basic physical and chemical concepts in material science.

V-M-1 Hydrogen-Exchange Reactions *via* Hot Hydrogen Atoms Produced in the Dissociation Process of Molecular Hydrogen on Ir{100}

MORITANI, Kousuke¹; OKADA, Michio¹;
NAKAMURA, Mamiko¹; KASAI, Toshio²;
MURATA, Yoshitada³

(¹Osaka Univ.; ²IMS and Osaka Univ.; ³Univ. Electro-Commun.)

[*J. Chem. Phys.* **115**, 9947 (2001)]

Adsorption of hydrogen(deuterium) on Ir{100} surface has been studied with temperature-programmed desorption and direct measurements of describing molecules using quadrupole mass spectrometry at ~ 100 K. H₂ exposure of the D-pre-covered Ir{100} surface was found to induce the desorption of HD and D₂ molecules. This result can not to be explained by conventional simple adsorption/desorption kinetics and it suggests that energetic H atoms (hot H atoms) produced in the dissociation process of incident H₂ molecules react with pre-adsorbed D atoms and then desorb as HD molecules or produces secondary energetic D atoms via energy transfer. Secondary energetic D atoms also induce associative reactions with pre-adsorbed D atoms and desorb as D₂ molecules. We propose the hot-H-atom-mediated reaction based on both empirical and steady-state approximation models for interpreting the present experimental results.

V-N Simulation of Molecular Clusters

Monte Carlo simulation is a powerful method for studying soft matter such as polymer, gel and biological molecules. We performed the structure analysis of chemical gel and characterized gel with cross-linkers. For vesicles, we studied self-assembly, fusion, adhesion and structural changes due to mechanical forces. In both systems, we obtained qualitatively good agreement with experimental results, and gave some insights to the mechanism of order formation of soft matter.

V-N-1 Characterization of Gel Using Modeled Radical Polymerization with Cross Linkers Performed by Monte Carlo Method

NOSAKA, Makoto¹; TAKASU, Masako¹; KATOH, Kouichi²

(¹IMS and Kanazawa Univ.; ²Kanazawa Univ.)

[*J. Chem. Phys.* **115**, 11333 (2001)]

In this study, some physical quantities for characterization of gel are proposed. Polymer networks (gel) are investigated by Monte Carlo simulation using modeled free-radical cross-linked polymerization in continuous system. The distributions of degree of polymerization for clusters obtained in this simulation show qualitatively good agreement with the experimental results. Linkers are classified to two types according to the roles in networks, and their ratios are discussed. The normal and weighted ratios of gel are defined using percolation theory. These ratios are compared with the changes in distribution.

V-N-2 Analysis of Intra- and Inter-Linkers in Gels by Brownian Dynamics Simulation

NOSAKA, Makoto¹; TAKASU, Masako¹

(¹IMS and Kanazawa Univ.)

The process of gelation was analyzed by Brownian dynamics simulation using modeled radical polymerization with cross-linkers. Particle densities were set near the gelation threshold determined experimentally (monomer density $d = 200$ mM 400 mM and 600 mM). We performed simulations under two conditions that did (Rule D) and did not (Rule A) prohibit the formation of intra-linkers. With Rule D, we observed gelation at $d = 600$ mM, and clustering at $d = 400$ mM. On the other hand, with Rule A, we did not observe gelation with any of the densities tested. We only observed clustering at $d = 600$ mM. Some quantities were investigated by comparing the results under the two conditions.

V-N-3 Self-Assembly of Amphiphiles into Vesicles: a Brownian Dynamics Simulation

NOGUCHI, Hiroshi; TAKASU, Masako¹

(¹IMS and Kanazawa Univ.)

[*Phys. Rev. E* **64**, 041913 (2001)]

We studied the vesicles of amphiphilic molecules using a Brownian dynamics simulation. An amphiphilic molecule is modeled as the rigid rod, and the hydro-

phobic interaction is mimicked by the local density potential of the hydrophobic particles. The amphiphilic molecules self-assemble into vesicles with bilayer structure. The vesicles are in fluid phase, and we calculated the lateral diffusion constant and the rate of the flip-flop motion of molecules in vesicles. The self-assembly kinetics into vesicles was also investigated.

V-N-4 Fusion Pathways of Vesicles, a Brownian Dynamics Simulation

NOGUCHI, Hiroshi; TAKASU, Masako¹

(¹IMS and Kanazawa Univ.)

[*J. Chem. Phys.* **115**, 9547 (2001)]

We studied the fusion dynamics of vesicles using a Brownian dynamics simulation. Amphiphilic molecules spontaneously form vesicles with a bilayer structure. Two vesicles come into contact and form a stalk intermediate, in which a necklike structure only connects the outer monolayers, as predicted by the stalk hypothesis. We have found a new pathway of pore opening from stalks at high temperature: the elliptic stalk bends and contact between the ends of the arc-shaped stalk leads to pore opening. On the other hand, we have clarified that the pore-opening process at low temperature agrees with the modified stalk model: a pore is induced by contact between the inner monolayers inside the stalk.

V-N-5 Adhesion of Nanoparticles to Vesicles: a Brownian Dynamics Simulation

NOGUCHI, Hiroshi; TAKASU, Masako¹

(¹IMS and Kanazawa Univ.)

[*Biophys. J.* **83**, 299 (2002)]

We studied the interaction of bilayer vesicles and adhesive nanoparticles using a Brownian dynamics simulation. The nanoparticles are simple models of proteins or colloids. The adhering nanoparticle induces the morphological change of the vesicle: budding, formation of two vesicles in which only outer monolayers are connected, and fission. We also show that the nanoparticle promotes the fusion process: fusion-pore opening from a stalk intermediate, a neck-like structure that only connects outer monolayers of two vesicles. The nanoparticle bends the stalk, and induces the pore opening.

V-N-6 Structural Changes of Pulled Vesicles: a Brownian Dynamics Simulation

NOGUCHI, Hiroshi; TAKASU, Masako¹
(¹IMS and Kanazawa Univ.)

[*Phys. Rev. E* **65**, 051907 (2002)]

We studied the structural changes of bilayer vesicles induced by mechanical forces using a Brownian dynamics simulation. Two nanoparticles, which interact repulsively with amphiphilic molecules, are put inside a vesicle. The position of one nanoparticle is fixed, and the other is moved by a constant force as in optical-trapping experiments. First, the pulled vesicle stretches into a pear or tube shape. Then the inner monolayer in the tube-shaped region is deformed, and a cylindrical structure is formed between two vesicles. After stretching the cylindrical region, fission occurs near the moved vesicle. Soon after this the cylindrical region shrinks. The trapping force ~ 100 pN is needed to induce the formation of the cylindrical structure and fission.

V-O Development of Broadband Solid-State NMR Spectroscopy

There are two different fields of solid-state NMR. One is biological, chemical and polymer NMR and the other is magnetic or metallic NMR. The former NMR employs resonant-type NMR probes, which can be tuned only over bandwidth of a few 100 kHz. Nuclear spins are controlled very precisely by sculpted RF pulse sequences. The unambiguous assignments of the lines are possible by using chemical shifts and spin-spin or dipolar couplings. One big outcome is that NMR teaches us not only a local information of an observed nucleus, but also correlations between different nuclei. The NMR parameters offered challenging problems for quantum chemical calculations and are now well predictable. The commercialization promoted rapid developments of sophisticated instruments with high resolution and sensitivity and the developments seems to be almost completed. However, in magnetic or metallic samples, most NMR works have been focused on only local information, like Knight shifts, hyperfine couplings, and relaxation times. Two-dimensional correlation NMR seems to be unpopular for these samples.

In magnetic and metallic samples, usually resonance lines are much broader than the diamagnetic samples. Ordinary resonant type NMR probes have a narrow tuning range and are inconvenient. It is possible to observe the spectra by a magnetic field sweep and with a fixed carrier frequency. However, sometimes the magnetic properties depend on the strength of static magnetic field. For example, the chemical shift of conducting samples can be field dependent due to the de Haas-van Alphen Effect (more generally Aharonov-Bohm effect).^{1),2)} We may also need a broadband NMR probe for frequency sweep experiments for studying such a subject. For ferromagnetic samples, the sensitivity of NMR is enhanced because motions of nuclear spins are coupled with motions of a macroscopic magnetization or domain walls. Detuned coils have been often used in a frequency sweep spectrometer. However, if the sensitivity is optimized, it may be possible to observe small patterned films, where various domain structures were theoretically investigated.

Here we reexamined a transmission line NMR probe, which was proposed by Lowe and coworkers in 70s.^{3),4)} The probe is expected to work in a wide frequency range below a certain cut-off frequency. The circuit resembles to that of a low-pass filter, which consists of π sections with a coil and two capacitors. The characteristic impedance must be adjusted to cable impedance by choosing an appropriate capacitance value. Some numerical results have been described in a previous report. We extended the numerical works from flat transmission coils to cylindrical transmission coils, since the latter form was easier to produce by using tip capacitors.

When we have a broadband NMR probe, we also need a broadband RF generator. Adiabatic pulses may be very effective for this purpose. Other types of selective RF pulses may be also useful, when we excite only a part of a spectral region. Conventional rectangular pulses are inconvenient, since its excitation envelope extends over a wide frequency range. Pulse shaping is commonly employed in a solution state spectrometer. However, for solid samples, the modulation must be much faster than the solution. Even in many high-resolution solid state NMR works, a phase transient due to a fast RF switching have been ignored. Using a fast RF modulator can solve these problems and fast modulated RF pulses. It would be also an attractive subject how various forbidden transitions can be controlled by shaped RF pulses.

References

- 1) R.G. Goodrich, S. A. Khan and J.M. Reynolds, *Phys. Rev. B* **3**, 2379 (1971).
- 2) A. Kubo, "Field dependent chemical shift of mesoscopic samples," Bunshikoukou-toronnkai, Kobe, 3P091 (2002).
- 3) I. J. Lowe and M. Engelsberg, *Rev. Sci. Instrum.* **45**, 631 (1974).
- 4) I. J. Lowe and D. W. Whitson, *Rev. Sci. Instrum.* **48**, 268 (1977).

V-O-1 Numerical Simulations and Experiments on the Transmission Line Probe

KUBO, Atsushi¹; ICHIKAWA, Shinji²
(¹IMS and Kyoto Univ.; ²Toyama Science Museum)

Previously, we have reported the numerical simulations of flat transmission line coils. We extended the simulation to cylindrical transmission line coils and constructed NMR probes by using the cylindrical coils. Lowe and co-workers mentioned that flat coils have advantages of the construction and the RF field homogeneity. However, our numerical result showed the homogeneity of a cylindrical coil was comparable to that of a flat coil. The homogeneity was mainly caused by the reflections of RF at the both ends of the coil, where the characteristic impedance was different from

the value at the coil center. The RF field strength decreases as the carrier frequency increases, because there is a phase delay between neighboring coil sections. The

$$\nu_d^{\text{cylinder}} = (Z_0 / \pi^2 \mu_0 a) (p/a)^2$$

characteristic decay frequency is given by where Z_0 , p , and a are a characteristic impedance, a pitch, and a diameter of the coil. The resonance frequency of the observed nuclei must be smaller than ν_d^{cylinder} . This condition restricts the size of the coil. We wound coils with the size $a = 2.3$ mm and $p = 1.2$ mm. At first, we made probes with $Z_0 = 50 \Omega$. The RF field strength at 400 MHz (¹H) was determined to be 60 kHz in experiments and was calculated to be 40 kHz for an input RF power of 100 W. However, the RF field strength of the ²³Na experiments at 106 MHz was found

much weaker (11 kHz) both in the experiments and in the calculation. The RF field strength was improved by twice when Z_0 was decreased to 12.5Ω and $\lambda/4$ cable impedance transformers were inserted at both the input and the output ports. The bandwidth was reduced to 30 MHz if $\lambda/4$ cable transformers were used. It is still much larger than the bandwidth of the ordinary resonant probe.

There are still some rooms for a further implementation. Noise of NMR signals is determined by resistive components in a probe circuit. In a transmission line probe, one port of the probe is terminated by a load or a transmitter (or a receiver). RF switches connect and disconnect them. The noise may be mainly generated at the load. If the load is cooled or resistance at load is reduced by appropriate impedance transformations, the signal to noise ratio might be improved. An ideal load must generate no thermal noise and absorb the signal completely. It may be also attractive to use a superconductor for the NMR probe circuit. One big problem of superconducting NMR probes (mainly used MRI) is that the probe Q becomes too high. The bandwidth of the probe is typically about 40 kHz, which allows only the observation of solution-state ^1H signals. The transmission line probe has a fast recovery time as a coaxial cable if the impedance is properly matched with the feeding and the receiving cables. More flexible design of superconducting probes may be possible by using transmission lines.

tion technologies. If there are several users who are interested in our fast digital RF modulator, it may be possible to order a company, who has a soldering machine, to make the printed circuit boards.

V-O-2 Developments of Fast Digital RF Frequency Modulator

YOSHIDA, Hisashi; KUBO, Atsushi¹
(¹IMS and Kyoto Univ.)

We used a quadrature digital upconverter AD9857 (Analog Devices). This IC generates the carrier signals and mixes them with the modulation signals digitally, so that the modulated RF output ($f_0 + f_m$) is expected to be free from the leakage of the carrier frequency signals (f_0) and the counter-quadrature signals ($f_0 - f_m$), which are unavoidable in analog modulators. We added a memory module for supplying digital amplitude data to AD9857. The memory module contains a large SRAM (256k words) and small SRAMs (2k words) for storing series of shaped pulses, starting addresses, and numbers of data in a shaped pulse, respectively. The memory module is controlled by three external TTL signals. It can be used in either a single pulse mode or a CW mode. In the latter mode, a shaped pulse is repeated until the external TTL signal is turned to high. The other TTL signals are employed to initialize the start address and to trigger pulsing. For the details of the design, please contact with Mr. Yoshida in Equipment Development Center. Some fast ICs were only available in a TSSOP package (lead pitch 0.65 mm). Mr. Yoshida did quite elaborate soldering works. Although commercial fast function generators are available, it is quite expensive and is not so convenient for magnetic resonance experiments. It may also have some pedagogical merit to know the actual design of the modulator, since the RF modulation is commonly used in communication technologies, and is a prototype of optical communica-